Experimental Simulation Study on the Impact of Gas Lift on the Flowability of Offshore Heavy Oil

Jianfei Wei[1], Na Xu[2], Zhenxing Tan[1], Hao Chen[1], Hongxing Yuan[3], and Yonghai Gao[3](✉)

[1] COSL-EXPRO Testing Services (Tianjin) Co., Ltd., Tianjin 300457, China
[2] Research Institute of Oil Production Engineering, PetroChina Daqing Oilfield Limited Company, Daqing 163453, China
[3] School of Petroleum Engineering, China University of Petroleum (East China), Qingdao 266580, China
upcgaoyh@163.com

Abstract. Gas lift is a commonly used method for extracting heavy oil, which has the advantages of simple and reliable construction, free control of depth, and minimal damage to reservoirs. When applied in actual field conditions, there may be issues with accurately assessing oil well production, and the flow characteristics of wellbore fluids during gas lift for heavy oil still require further research. This study employs experimental methods to investigate the flow behavior of heavy oils with different viscosities during gas lift. In this context, 5# white oil, 68# white oil, and 300# white oil respectively represent low viscosity, medium viscosity, and high viscosity scenarios. Air injection is used to simulate the actual field injection of nitrogen. The experiments simulated the variations in wellbore friction pressure drop and total pressure drop under different gas injection rates and liquid flow rates for varying viscosity levels. It can be observed that as the viscosity of the crude oil increases, the impact of frictional pressure drops on the total pressure drop becomes more pronounced. Additionally, the study also examined the characteristics of bottom-hole pressure changes during the experimental process. Analysis of the experimental data indicates that reducing the gas injection rate at the beginning of the injection process can effectively mitigate the negative impact on bottom-hole pressure. Finally, utilizing the images of two-phase flow patterns captured during the experiments and the recorded data, flow regime maps were constructed for different viscosities. This will contribute to improving the accuracy of two-phase pressure drop calculations for highly viscous oil and gas flows.

Keywords: gas lift · offshore heavy oil · flowability · bottom-hole pressure · flow regime map

B. Sun et al. (Eds.): DWOG-Hyd 2023, LNCE 472, pp. 157–168, 2024.
https://doi.org/10.1007/978-981-97-1309-7_15

1 Introduction

As the world continues to develop rapidly, conventional and easily accessible oil and gas resources, being non-renewable, are gradually depleting. Consequently, the significance of heavy oil in the global petroleum resources is growing [1]. Due to its high viscosity, heavy oil typically cannot naturally flow to the surface using reservoir energy alone. Therefore, it requires the use of artificial methods to assist in its extraction. The commonly used methods for heavy oil extraction at present include screw pumps [2], jet pumps [3], gas lift [4], dilution [5], and electrical heating [6]. Gas lift for heavy oil, as one of these methods, offers advantages such as simplicity of operation, ease of control, high economic efficiency, and minimal reservoir damage [7]. However, during its application, gas lift for heavy oil has encountered issues related to the accurate assessment of well production. An analysis suggests that this may be attributed to the negative impact on bottom-hole pressure during the gas injection process, which consequently prevents the full realization of well productivity. Based on the reasons mentioned above, it is necessary to conduct research on the flowability of heavy oil in gas lift operations.

The study of the flowability of heavy oil in gas lift operations involves researching the flow characteristics of two-phase gas-liquid fluids. Currently, many scholars have conducted extensive research on the application of different two-phase pressure models in the context of high-viscosity liquid phase and gas. These researches are based on a substantial amount of laboratory experiments and field data analysis. Jeyachandra et al. [8] investigated the two-phase flow characteristics of high-viscosity oil and gas under various incline conditions, selecting four different oil viscosities of 0.585 Pa·s, 0.378 Pa·s, 0.257 Pa·s, and 0.181 Pa·s. They also assessed the corresponding flow regime maps and pressure drop data. Chung et al. [9] focused on the offshore heavy oil lifting process and set up experimental equipment for high-viscosity oil-gas systems with a 2-in. diameter experimental pipeline. They obtained data on pressure gradients, flow patterns, holdup rates, and more. They compared the experimental results with data from water-gas experiments and analyzed the differences between the experimental data and existing models. Al-Ruhaimani et al. [10] conducted research from both experimental and theoretical perspectives, investigating the differences in the upward vertical flow of high-viscosity and low-viscosity oil two-phase flow models. They tested viscosities as high as 586 mPa·s and compared their flow regime maps with theoretical models, demonstrating significant discrepancies in the predicted pressure drop for high-viscosity oil compared to traditional flow regime maps. Gan et al. [11] designed two-phase flow experiments to investigate the impact of different viscosities on the pressure of gas-liquid two-phase flow. They compared the experimental data with three empirical models: Begg-Brills, Hasan-Kabir, and Mukherjee-Brill. They found that as viscosity increased, the accuracy of the models gradually decreased. Among the three models, Begg-Brills exhibited higher accuracy compared to the others, but its error became significant when viscosity reached 200 mPa·s.

Most existing models are primarily based on experiments with light oil or water as the liquid phase. If directly applied to heavy oil, it can lead to significant deviations in the results. Moreover, there is a lack of highly accurate two-phase pressure models specifically tailored to high-viscosity and heavy oil systems. Based on the current situation, this study utilized experimental methods to investigate frictional pressure drop

and bottom-hole pressure changes under various conditions. Flow regime maps were also created for different viscosities, significantly enhancing the accuracy of two-phase pressure calculations for high-viscosity oil and gas systems.

2 Gas Lift Flowability Experiment

2.1 Experimental Procedure and Equipment

The experimental setup can be divided into three main components: data control and measurement system, gas-liquid supply system, and pipeline flow system (Fig. 1). Firstly, the experimental oil is pumped out through a screw pump after being heated in the oil storage tank, simulating the production of heavy oil from the reservoir. A liquid flow control valve is used to adjust the oil flow rate. Subsequently, the oil travels through the pipeline to reach the bottom of the wellbore. An air compressor compresses air, which is then controlled by a gas regulating valve to enter the bottom of the wellbore. After mixing at the well bottom, the liquid and gas flow vertically through the measurement pipeline within the experimental wellbore and exit from the top. The gas is released directly, while the liquid is recycled back to the oil storage tank for reuse.

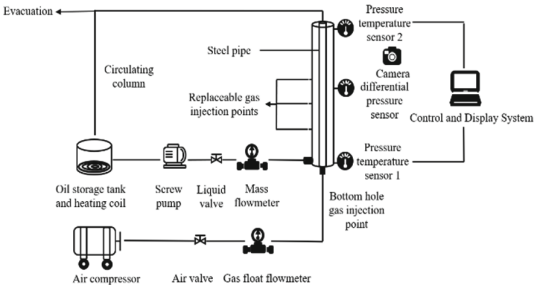

Fig. 1. Schematic of gas lift simulation experiment.

2.2 Experimental Materials and Apparatus

The materials required for the experiment include: (1) experimental liquids: white oil 5#, white oil 68#, white oil 300#; (2) experimental gas: air.

The experimental equipment and components include: air compressor, visualized simulated wellbore, liquid mass flow meter, liquid storage tank, pressure sensor, temperature sensor, gas float flow meter, liquid flow meter, screw pump, water bath and coil. The experimental flow pipeline system and equipment are as shown in Fig. 2.

The entire pipeline has a vertical height of 4 m and consists of an outer organic transparent glass tube and an inner steel tube, allowing for easy observation of gas-liquid flow patterns. At the bottom and top of the entire pipeline, temperature and pressure sensors are installed. Additionally, pressure differential sensors are positioned at the flange

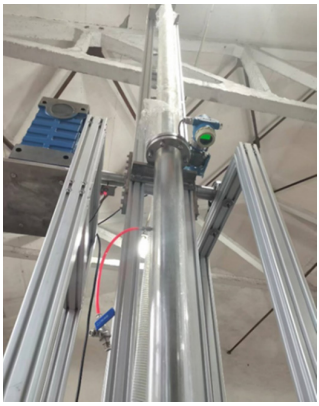

Fig. 2. Diagram of vertical flow visualization equipment.

connections of the outer organic glass tube to facilitate the measurement of pressure differentials along the pipeline. The organic glass tube has side openings for gas injection, allowing gas injection at various positions along the tube.

The experiment also features a central control system and real-time data acquisition capability. The system can be operated via an external display screen or connected to a computer, making it convenient to control and adjust the equipment for starting, stopping, setting motor operating frequencies, and configuring pipeline tilt angles, among other functions. Additionally, it can also record experiment pipeline temperature, pressure, pressure differentials, instantaneous liquid flow rates, cumulative flow rates, and the actual motor frequency.

2.3 Experimental Steps

The entire experimental process can be summarized as follows: Under specified liquid velocity conditions, the experiment involves altering different gas velocities to measure upper-end pressure, lower-end pressure, flow patterns, and holdup in the wellbore. Subsequently, the liquid velocity, liquid viscosity, gas injection location, and other parameters are varied, and the above measurements are repeated. Each set with the same liquid quantity is considered as one group. The specific experimental procedure is as follows:

(1) Check the airtightness of the experimental pipeline and equipment. Verify that all instruments are set to their initial values and that the display monitor connections are functioning properly. Open all valves in the loop to ensure that the entire system is unobstructed;
(2) Fill the liquid storage tank, turn on the liquid pump and water bath, and gradually increase the flow rate. Allow the liquid to circulate, cleaning the pipeline and the experimental wellbore. After approximately 10 min, stop the circulation;
(3) Set a specific liquid flow rate and record it. Then, open the air compressor, adjust the gas injection valve, and record the gas flow rate;

(4) Continuously record the lower-end pressure, upper-end pressure, and pressure differential in the wellbore while observing and capturing images of the flow patterns within the pipeline;
(5) Simultaneously close the lower-end gas valve and liquid valve, let it stand for 2 min, then measure the liquid height (L) in the vertical pipeline, and calculate the holdup rate;
(6) Reopen the liquid injection valve, change the gas flow rate, and repeat steps (4) to (5);
(7) Change the liquid flow rate, viscosity, gas injection location, and repeat steps (3) to (6).

3 Experimental Results and Discussion

By observing the experimental phenomena, recording experimental data, and summarizing the relevant patterns, the analysis is conducted as follows for different viscosity white oils.

3.1 Analysis of Pressure Drop with Different Viscosities

The experiment conducted pressure drop relationship measurements for 5#, 68#, and 300# white oils under different conditions, as shown in Figs. 3, 4, and 5.

Figures 3, 4, and 5 respectively represent the variations of pressure drop gradient with gas flow rate for 5#, 68#, and 300# white oils at liquid flow rates of 0.76 $m^3 \cdot h^{-1}$, 1 $m^3 \cdot h^{-1}$, 1.5 $m^3 \cdot h^{-1}$, and 2 $m^3 \cdot h^{-1}$. Under the experimental conditions, three flow patterns were observed: bubbly flow, slug flow, and annular flow. However, the annular flow pattern was not observed in this experiment, likely due to the influence of the experimental equipment. Acceleration pressure drop is typically significant only in mist flow [12], so it is considered that the total pressure drop is composed of gravitational pressure drop and frictional pressure drop.

From the graph, it can be observed that at a constant liquid injection rate, when the gas flow rate is relatively low, whether it's low-viscosity or high-viscosity oil, the gravitational pressure drop consistently accounts for a larger proportion of the total pressure drop compared to the frictional pressure drop. When the gas injection rate is held constant, increasing the liquid flow rate leads to a larger total pressure drop, while the frictional pressure drop decreases. Comparing 5#, 68#, and 300# white oils, it can be observed that as the viscosity of the crude oil increases, the impact of frictional pressure drop on the total pressure drop becomes more pronounced. Therefore, in the calculation process of the high-viscosity oil-gas two-phase pressure model, it is important to pay attention to the influence of frictional pressure drop.

3.2 Analysis of Bottom-Hole Pressure Fluctuation

In order to observe the characteristics of bottom-hole pressure changes during the experimental process, pressure fluctuations at the bottom of the column were recorded by sensors during the initial gas injection phase. Analysis revealed that during the initial entry

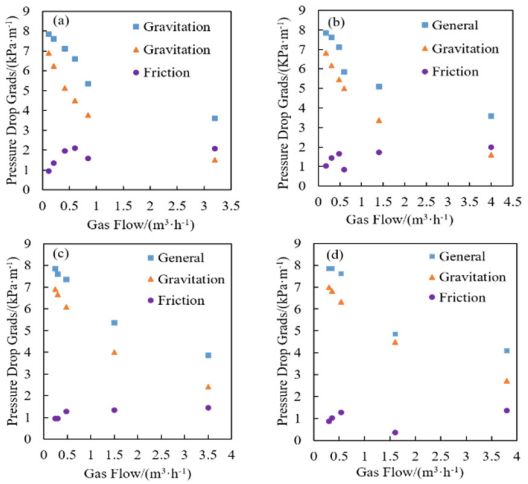

Fig. 3. Pressure drop gradient of 5# white oil under different liquid flow rates: (a) 0.76 $m^3 \cdot h^{-1}$; (b) 1 $m^3 \cdot h^{-1}$; (c) 1.5 $m^3 \cdot h^{-1}$; (d) 2 $m^3 \cdot h^{-1}$.

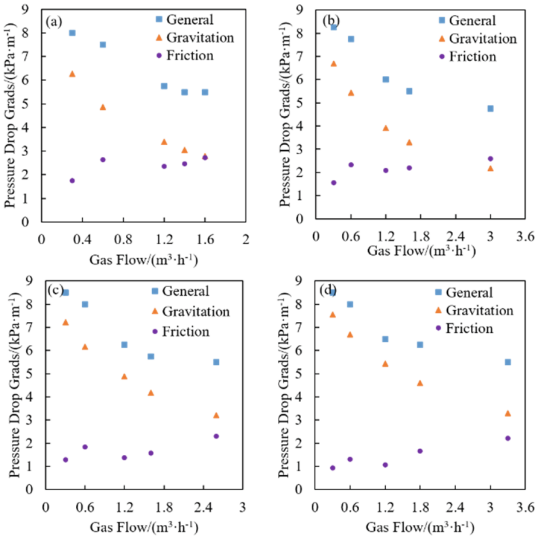

Fig. 4. Pressure drop gradient of 68# white oil under different liquid flow rates: (a) 0.76 $m^3 \cdot h^{-1}$; (b) 1 $m^3 \cdot h^{-1}$; (c) 1.5 $m^3 \cdot h^{-1}$; (d) 2 $m^3 \cdot h^{-1}$.

of gas into the column, the bottom-hole pressure does not decrease due to the reduced column density. Instead, it initially increases, then decreases, and eventually stabilizes over a short period of time. In practical engineering, to fully understand the principles of gas lift injection, it is important to clarify whether injecting gas into the wellbore and its contact with the reservoir-produced fluid have any negative effects on the bottom-hole conditions. Based on the above questions, record the bottom-hole pressure fluctuations

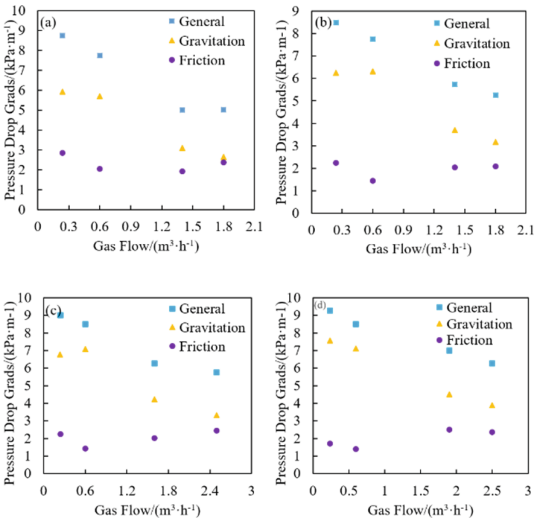

Fig. 5. Pressure drop gradient of 300# white oil under different liquid flow rates: (a) 0.76 $m^3 \cdot h^{-1}$; (b) 1 $m^3 \cdot h^{-1}$; (c) 1.5 $m^3 \cdot h^{-1}$; (d) 2 $m^3 \cdot h^{-1}$.

during the initial gas injection phase for 5#, 68#, and 300# white oils under different conditions. Plot the pressure fluctuation curves and analyze the patterns of bottom-hole pressure fluctuations, as shown in Figs. 6 and 7.

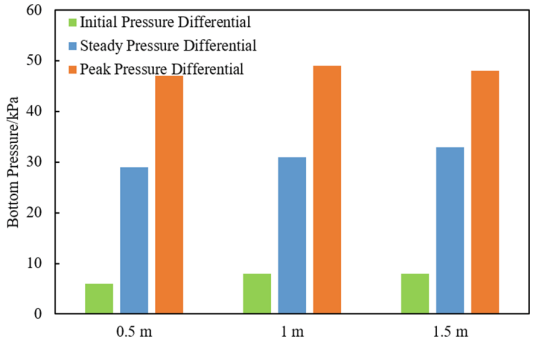

Fig. 6. Pressure fluctuation at the bottom of the pipe at different injection heights.

Figure 6 represents the pressure fluctuation characteristics under the same gas injection conditions at distances of 0.5 m, 1 m, and 1.5 m from the bottom of the wellbore. With the same liquid injection rate, the initial bottom-hole pressure is the same. Therefore, the impact of different gas injection positions on bottom-hole fluctuations can be represented through the pressure differential data of the column. During the initial gas injection phase, although injecting gas reduces the density of the column's fluid, bottom-hole pressure does not immediately decrease. This is because the fluid mixing velocity within the column increases, leading to a rapid increase in frictional pressure.

As a result, bottom-hole pressure experiences a sudden peak before stabilizing. However, the increase in frictional pressure caused by the upper fluid during gas injection quickly becomes smaller than the reduction in gravitational pressure drop after gas-liquid mixing. As a result, bottom-hole pressure gradually decreases and stabilizes over time. Observing Fig. 6, it can be noted that changing the gas injection position has a relatively minor effect on the trend and peak variation of bottom-hole pressure fluctuations.

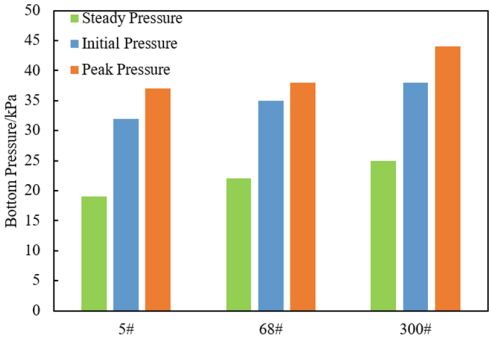

Fig. 7. Pressure fluctuation at the bottom of the pipe with different white oil viscosities.

Figure 7 represents the bottom-hole pressure fluctuation characteristics for three viscosity grades of white oil under the same liquid and gas injection conditions when the gas injection point is at the bottom of the wellbore. Combining the observed phenomena during the experiment and the analysis of experimental data, it is found that: The time at which peak values occur differs among white oils with different viscosities, with higher viscosity white oils exhibiting longer peak times; the fluctuation pressures at the start are similar for white oils with different viscosities.

In the experiment, it was also observed that the peak values of bottom-hole pressure fluctuations are influenced by the gas injection velocity. If the gas instantly reaches the specified gas volume, significant pressure fluctuations occur. However, once the gas flow stabilizes, the bottom-hole pressure approaches stability as well. Additionally, a faster gas injection rate leads to greater fluctuations in pressure. If the gas velocity is slowly adjusted, the pressure peaks approach the initial pressure, resulting in a smaller negative impact on bottom-hole pressure. Based on the research mentioned above, it is believed that reducing the gas injection rate at the start of the gas injection process can effectively mitigate the negative impact on bottom-hole pressure.

3.3 Analysis of Flow Patterns with Different Viscosities

Observing and photographing the two-phase flow patterns, differentiating them for 5#, 68#, and 300# white oils under different gas-liquid flow rates, it was found that white oils with different viscosities exhibit significant differences in bubbly flow and slug flow patterns under the same gas and liquid flow conditions. The three observed flow patterns for the different white oils are shown in Figs. 8 and 9.

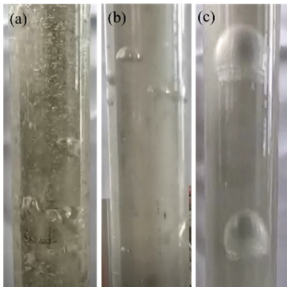

Fig. 8. Flow morphology of bubble flow in different types of white oil: (a) 5#; (b) 68#; (c) 300#.

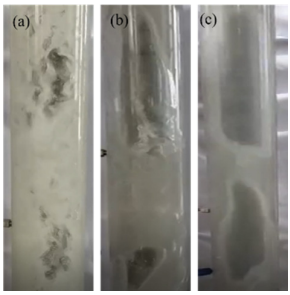

Fig. 9. Flow morphology of slug flow in different types of white oil: (a) 5#; (b) 68#; (c) 300#.

Based on the experimental findings, it was observed that there are significant differences in the boundaries of two-phase flow patterns for different viscosities. The specific flow pattern divisions are shown in Figs. 10, 11, and 12.

Analyzing Figs. 8, 9, and 10, it can be observed that when the fluid is in a bubbly flow pattern, small bubbles are dispersed extensively in the pipeline. However, the bubble sizes are not uniform, and some small bubbles collide and aggregate to form larger bubbles. Large bubbles, influenced by buoyancy, move at a higher velocity and continue to come into contact with, squeeze, and merge with the bubbles above. During flow, the bubbles frequently undergo deformation, making it difficult to form a regular slug flow pattern. In the slug flow pattern, there is alternating appearance of gas and liquid, and under the influence of gravity, gas-liquid slip increases. Gas velocity continues to increase, and the liquid tends to adhere to the inner and outer pipe walls within the annular space.

Analyzing Figs. 8, 9, and 11, it can be observed that compared to 5# white oil, the increased viscosity of 68# white oil leads to a significant reduction in the number of small bubbles during the bubbly flow stage. Due to viscosity effects, gas tends to aggregate and form larger bubbles, resulting in a decrease in the number of bubbles inside the pipeline. As the gas content continues to increase, the bubbles at the rear catch up with the ones in front, forming a regular slug flow pattern within the annular pipe. At the same time, as the liquid viscosity increases and intermolecular forces become stronger, the liquid phase is less likely to be disrupted by the gas phase. This is reflected in the flow pattern

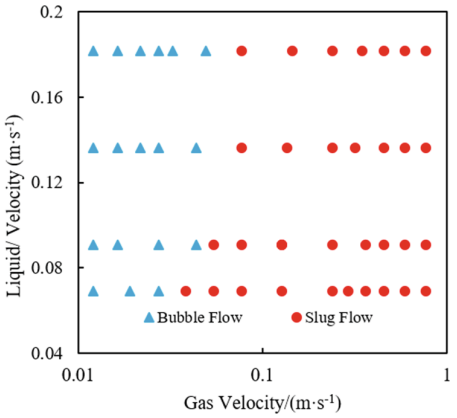

Fig. 10. The flow pattern diagram of 5# white oil.

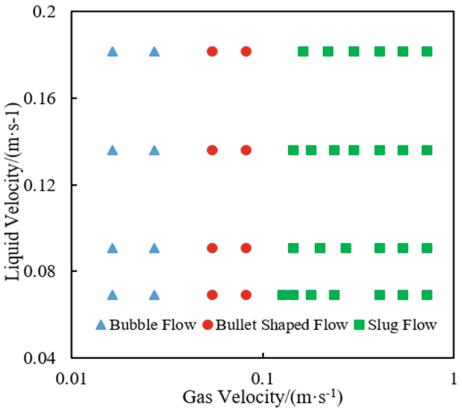

Fig. 11. The flow pattern diagram of 68# white oil.

by a narrowing of the slug flow range and an expansion of the slug flow range within the diagram.

Analyzing Figs. 8, 9, and 12, it can be observed that in the bubbly flow stage, 300# white oil tends to form bubbles that are closer to a slug flow pattern. Small bubbles are rarely observed within the pipeline, and the slug-like bubble range is larger with a higher occurrence rate. This gas aggregation effect is also evident in the slug flow stage, where large continuous gas phases are more likely to appear, and there are fewer bubbles in the liquid slug segment.

5#, 68#, 300# white oils respectively represent low viscosity, medium viscosity, and high viscosity fluids, and they exhibit significant differences in flow patterns under different apparent gas velocities and liquid velocities. Comparing Figs. 10, 11, and 12, it can be seen that as viscosity increases, the number of small bubbles decreases, and gas tends to aggregate, forming a regular slug flow pattern. The range of slug flow patterns further expands with increasing viscosity. Observations from Figs. 8 and 9 reveal that

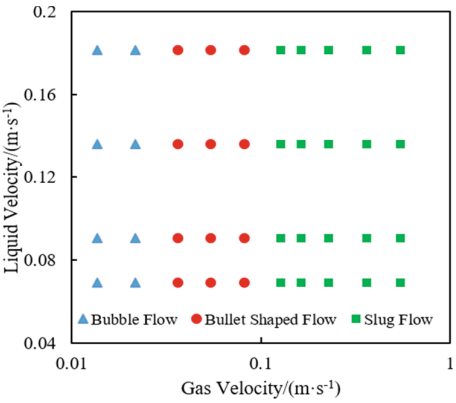

Fig. 12. The flow pattern diagram of 300# white oil.

during the experiment, compared to low-viscosity oil, high-viscosity oil has stronger intermolecular forces, which make the bubbles less prone to breaking and more likely to aggregate and form larger bubbles. However, commonly used two-phase gas-liquid models often choose low-viscosity oil or water as the experimental fluid, which can lead to a decrease in the accuracy of pressure drop calculations for high-viscosity oil.

4 Conclusion

This paper conducted research on the flow characteristics of heavy oil using gas lift through experimental methods. It analyzed the variations in pressure drop, flow patterns, and bottom-hole pressure fluctuations for different viscosity white oils. By utilizing experimental data, flow pattern maps were generated for different viscosities, improving the accuracy of pressure drop calculations for gas-liquid two-phase flow in high-viscosity oil. This provides valuable insights for the precise calculation of pressure drops in heavy oil wellbores.

(1) Comparing the three types of white oil, it can be observed that as the viscosity of crude oil increases, the impact of frictional pressure drops on the total pressure drop becomes more pronounced. Therefore, in the calculation process of high-viscosity oil-gas two-phase pressure models, it is important to consider the influence of frictional pressure drop.
(2) The peak of bottom-hole pressure fluctuations is influenced by the gas injection rate. Lowering the gas injection rate at the start of the gas injection process can effectively reduce the negative impact on bottom-hole pressure.
(3) Commonly used gas-liquid two-phase flow pattern maps mainly use low-viscosity oil or water as experimental fluids, resulting in lower accuracy when calculating two-phase flow pressure drops. The high-viscosity oil-gas two-phase flow pattern maps proposed in this paper effectively address this issue.

Acknowledgement. The authors would like to appreciate the support from the National Natural Science Foundation of China (No. U21B2065, No. 52274022).

References

1. Chen, H.B., Yang, L.: The strategic selection for the exploitation and utilization of oil and gas resources under the background of "Double Carbon" goals and energy security in China. Urban Environ. Stud. **33**(03), 56–69 (2022)
2. Song, H.Q.: Application of electric submersible screw pumps in offshore tight oil fields. Inner Mongolia Petrochem. Ind. **36**(02), 24–25 (2010)
3. Zong, F.C., Qi, T., Li, W.C., et al.: Viscosity reducing and integrated artificial lift techniques for heavy oil wellbore in offshore oilfield. Oil Drill. Prod. Technol. **33**(03), 47–50 (2011)
4. Ning, B., Wu, Y.L., Li, J.J., et al.: Application status of gas lift technology in heavy oil recovery. China Petrol. Chem. Ind. **298**(12), 53–55 (2015)
5. Guo, J.X., Zhang, J.W.: Review on the technology of blending diluting oil in heavy oil well. Sci. Technol. Eng. **14**(36), 124–132 (2014)
6. Tang, G.Q., Xiong, Y.M., Wang, Y.M., et al.: Research on electrical heating viscosity breaking craft for Huate Mer A deepwater heavy oil fields. Oil Field Equip. **44**(03), 55–59 (2015)
7. Zhang, Y., Luo, D.: Analysis of the application of continuous tubing technology in underground operations. Chem. Eng. Manag. **566**(23), 161–162 (2020)
8. Jeyachandra, B.C., Sarica, C., Zhang, H.Q., et al.: Inclination effects on flow characteristics of high viscosity oil/gas two-phase flow. SPE159217 (2012)
9. Chung, S., Pereyra, E., Sarica, C., et al.: Effect of high oil viscosity on oil-gas flow behavior in vertical downward pipes. BHR-2016-259 (2016)
10. Al-Ruhaimani, F., Pereyra, E., Sarica, C., et al.: Experimental analysis and model evaluation of high-liquid-viscosity two-phase upward vertical pipe flow. SPE J. **22**(03), 712–735 (2017)
11. Gan, Q.M., Lei, Y., Wu, Z.H., et al.: The influence of viscosity on pressure drop of gas-liquid two-phase flow in vertical pipe. Sci. Technol. Eng. **19**(19), 134–142 (2019)
12. Zhang, X.H., Fang, Z.G., Tang, A.D., et al.: Research on two-phase flow experiment and pressure drop model of higher viscosity oil in vertical pipe. China Sciencepaper **15**(07), 755–760 (2020)